Liao, Mengzhou; Nicolini, Paolo; Du, Luojun; Yuan, Jiahao; Wang, Shuopei; Yu, Hua; Tang, Jian; Cheng, Peng; Watanabe, Kenji; Taniguchi, Takashi; Gu, Lin; Claerbout, Victor E.P.; Silva, Andrea; Kramer, Denis; Polcar, Tomas; Yang, Rong; Shi, Dongxia; Zhang, Guangyu

Ultra-low friction and edge-pinning effect in large-lattice-mismatch van der Waals heterostructures

Published in:
Nature Materials

DOI:
10.1038/s41563-021-01058-4

Published: 01/01/2022

Document Version
Peer-reviewed accepted author manuscript, also known as Final accepted manuscript or Post-print

Please cite the original version:
Liao, M., Nicolini, P., Du, L., Yuan, J., Wang, S., Yu, H., Tang, J., Cheng, P., Watanabe, K., Taniguchi, T., Gu, L., Claerbout, V. E. P., Silva, A., Kramer, D., Polcar, T., Yang, R., Shi, D., & Zhang, G. (2022). Ultra-low friction and edge-pinning effect in large-lattice-mismatch van der Waals heterostructures. *Nature Materials*, *21*(1), 47-53. https://doi.org/10.1038/s41563-021-01058-4

Ultra-low friction and edge-pinning effect in large-lattice-mismatch van der Waals heterostructure

Mengzhou Liao[1,2], Paolo Nicolini[2], Luojun Du[1,3], Jiahao Yuan[1,4], Shuopei Wang[1,9,a], Hua Yu[1,4], Jiang Tang[1,4], Peng Cheng[5], Kenji Watanabe[6], Takashi Taniguchi[6], Lin Gu[1,4], Victor E. P. Claerbout[2], Andrea Silva[7], Denis Kramer[7, 8], Tomas Polcar[2, 7], Rong Yang[1, 9,a], Dongxia Shi[1,4,9] and Guangyu Zhang[1,4,9,a*]

[1] *Beijing National Laboratory for Condensed Matter Physics and Institute of Physics, Chinese Academy of Sciences, Beijing 100190, China*

[2] *Department of Control Engineering, Faculty of Electrical Engineering, Czech Technical University in Prague, Technicka 2, 16627 Prague 6, Czech Republic*

[3] *Department of Electronics and Nanoengineering, Aalto University, Tietotie 3, FI-02150, Finland*

[4] *School of Physical Sciences, University of Chinese Academy of Sciences, Beijing 100190, China*

[5] *Oxford Instruments (Shanghai) Co. Limited, Shanghai 201109, China*

[6] *National Institute for Materials Science, 1-1 Namiki, Tsukuba 305-0044, Japan*

[7] *National Centre for Advanced Tribology Study at University of Southampton, Southampton SO171BJ, United Kingdom*

[8] *Faculty of Mechanical Engineering, Helmut Schmidt University, 22043, Hamburg, Germany*

[9] *Beijing Key Laboratory for Nanomaterials and Nanodevices, Beijing 100190, China*

[a] *Songshan Lake Materials Laboratory, Dongguan, Guangdong 523808, China*

* Corresponding author. E-mail: gyzhang@iphy.ac.cn (G.Z.)

Abstract

Two-dimensional heterostructures are excellent platforms to realize twist-angle independent ultra-low friction due to their weak interlayer van der Waals interactions and natural lattice mismatch. However, for finite-size interfaces, the effect of domain edges on the friction process remains unclear. Here, we report on the superlubricity phenomenon and the edge pinning effect at MoS_2/graphite

and MoS_2/h-BN van der Waals heterostructure interfaces. We find that friction coefficients of these heterostructures are below 10^{-6}. Molecular dynamics simulations corroborate experiments highlighting the contribution of edges and interface steps to friction forces. Our experiments and simulations provide more information on the sliding mechanism of finite low-dimensional structures, which is vital to understand the friction process of laminar solid lubricants.

Introduction

Friction causes massive energy dissipation and mechanical abrasion between machine component parts in the world every year[1,2]. Understanding the mechanism of the frictional processes and searching for an optimum material combination, ideally providing a near frictionless state, is thus essential. The concept of superlubricity was proposed by K. Shinjo and M. Hirano in the 1990s[3], which describes the phenomenon of vanishing friction between two contact surfaces. Superlubricity has been widely found in van der Waals (vdW) materials, as their crystalline structures are kept together by weak vdW forces[4]. However, superlubricity in two dimensional (2D) homostructures shows a strong twist-angle dependence[5-7]. Layers prefer to rotate and lock in the commensurate state when sliding occurs, leading to the disappearance of superlubricity[6,8]. VdW heterojunctions may reduce the commensuration problem since the lattice mismatch between the two contact materials will come into play. Micro-scale superlubricity has been uncovered in the graphene/hexagonal boron nitride (h-BN) heterostructure with a significant reduction of twist-angle dependence[9-11]. However, the twist-angle dependence is still present in graphene/h-BN heterostructure, perhaps due to the small lattice mismatch. Thus, it is crucial to explore the lattice mismatch influence on the superlubricity of 2D heterostructures. Furthermore, the effect of widespread domain edges and interface steps on the superlubricity of the finite-size 2D interfaces may prevent superlubricity.

In this work, we characterized 2D heterojunction interfaces with different lattice mismatches: molybdenum disulfide (MoS_2) /graphite, MoS_2/h-BN, and graphene/h-BN by Lateral Force Atomic Force Microscope (LF-AFM). Our results show that the coefficient of friction of the large lattice mismatch MoS_2/graphite and MoS_2/h-BN heterojunction interfaces is below $10^{-6,}$ and twist-angle dependence is suppressed. We demonstrate that the friction forces of these two heterojunctions are dominated by

pinned edges or substrate steps effects rather than resistance to interface sliding, from e.g. potential energy corrugation. We also measured graphene/h-BN, a heterojunction with a small lattice mismatch, for comparison. Interface sliding resistance still dominates the friction process. Classical molecular dynamics (MD) simulations indicate that atoms near the edges of the flake play a distinctive role during the sliding dynamics, presenting enhanced structural distortions with respect to the rest of the flake. Given the non-reactive nature of the force fields employed in the MD simulations, we also indirectly prove that dangling bonds at the edge of the domains contribute mostly to the friction force observed in climbing substrate steps.

Results

Growth and characterization of vdW heterostructures

VdW heterostructure samples investigated in this work include MoS_2/graphite, MoS_2/h-BN, and graphene/h-BN with lattice mismatches of 26.8%, 24.6%, and 1.8%, respectively. Figs. 1**a-c** show the structures of these three heterostructures. All samples were prepared by an epitaxial growth technique described in our previous works[12-14]. (see the Methods section for more details). Figs. 1**d**–**f** show typical AFM topographic images; these epitaxial interfaces are ultra-clean. The heights of monolayer MoS_2 on graphite and h-BN are 0.83 nm and 0.72 nm, respectively, and the height of monolayer graphene on h-BN is 0.35 nm, all in agreement with previous reports[14,15]. We used selected area electron diffraction (SAED) to characterize the lattice alignment of our MoS_2/graphite and MoS_2/h-BN heterostructures. As illustrated in Fig. S1**b** and 1**e**, the hexagonal diffraction spots of both MoS_2 and graphite (h-BN) have the same orientation, indicating either 0° or 60° twisting angle between the as-grown MoS_2 and graphite (h-BN) substrate. Fig. S1**h** shows that the period of the moiré superlattice of as-grown graphene/h-BN heterostructure is ~16 nm, also suggesting a 0°twist angle. Raman and photoluminescence (PL) spectra in Fig. S1**c** and 1**f** also demonstrate a high sample quality. For more information, please refer to Supplementary Note 1.

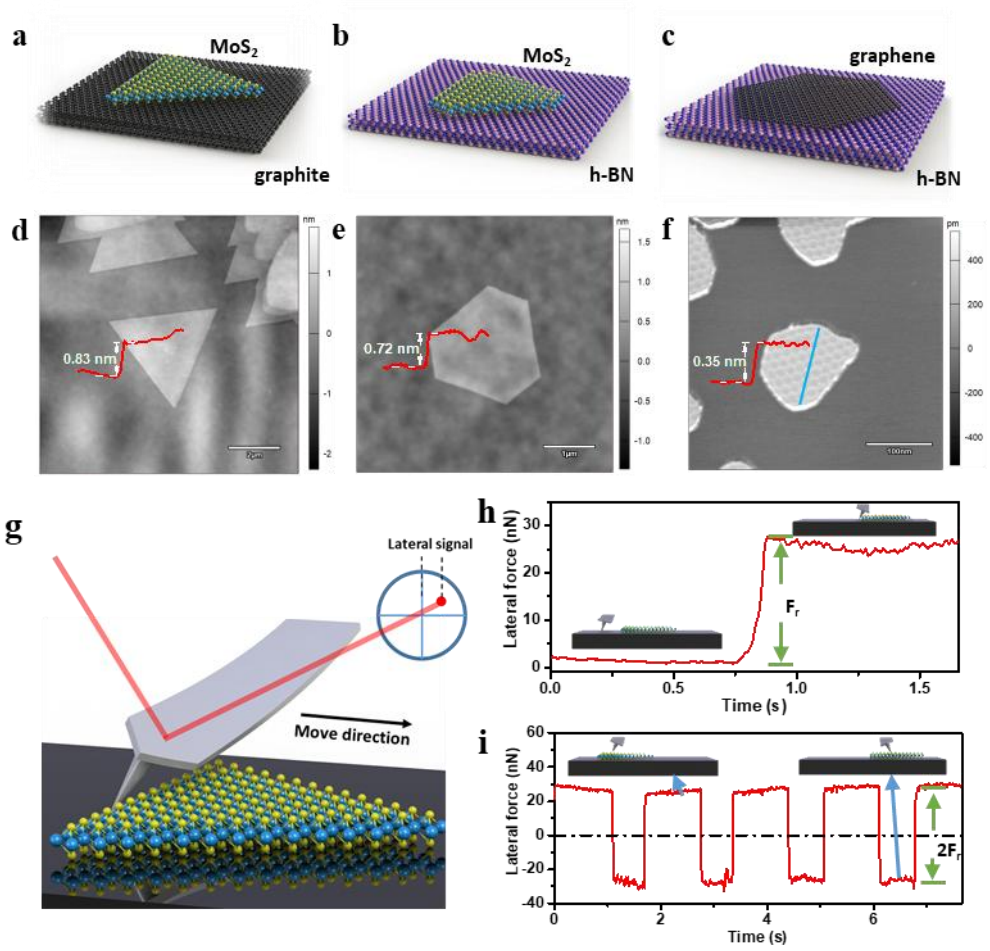

Fig. 1 | Friction characterizations of 2D heterostructures. a-c Atomic structures and **d-f** AFM images of three heterostructures: MoS_2/graphite, MoS_2/h-BN, and graphene/h-BN, respectively. **g** Diagram of friction force measurements. **h** and **i** Two different strategies for friction force characterizations of MoS_2/graphite and MoS_2/h-BN heterostructures: **h** by pushing from the edge of domain, or **i** by dragging with the tip placed at the center of the domain, the sign of the force indicates the sliding direction.

Superlubricity behavior of vdW heterostructures

We performed friction force measurements by AFM in dry N_2 atmosphere and under ambient conditions. Fig. 1**g** shows a schematic of our measurements process. Based on a manipulation technique we developed previously[11,16], we can slide atop epitaxial domains on the substrate by using an AFM tip and monitor the lateral force during the sliding simultaneously. (please refer to the Methods section and Supplementary Note 2 for more details). In the experiment, we explore two approaches to slide on-top domains on substrates by using AFM tips. The first is illustrated in Fig. 1**h**, where we laterally push the edge of the top domain and detect the difference of lateral force before and after on-top domain sliding. The second way

is shown in Fig. 1**i.** For MoS_2/graphite and MoS_2/h-BN heterostructures, we could slide the top domains back and forth laterally by engaging the tip onto the center of the domain, with a load from 0.4 to 5μN, since the friction force between the tip and MoS_2 is much greater than that between MoS_2 and graphite (or h-BN).

According to Amontons' law, the dependence of the friction force F_r on the load L is expressed by

$$F_r = \mu \cdot L,$$

where μ is the coefficient of friction (COF). By taking advantage of both approaches, we can change the applied tip load L_{tip} from zero to a few μN (zero tip load achieved by pushing the edge). The normal force experienced by the flake can be decomposed into two contributions

$$L = L_0 + L_{tip},$$

with L_0 being the adhesion between MoS_2 and graphite (or h-BN) and L_{tip} the load applied to the tip. It follows that:

$$F_r = \mu \cdot (L_0 + L_{tip}) = \mu \cdot L_0 + \mu \cdot L_{tip} = F_{r0} + \mu \cdot L_{tip}.$$

As shown in Fig. 2**a** and **b**, under N_2, the friction forces of MoS_2/graphite and MoS_2/h-BN heterostructures are almost the same for different values of L_{tip}, which indicates constant F_{r0} and ultralow COF. As shown in Fig. 2, the coefficient of friction of both MoS_2/graphite and MoS_2/h-BN heterostructure interfaces is well below 10^{-3}, which is considered the threshold for superlubricity[17]. To calculate the friction coefficient precisely from the slope in Fig 2**a** and **b**, a much higher resolution and noise reduction of the AFM signal would be needed.

Nevertheless, we can use an alternative approach to estimate the COF. The adhesive force between MoS_2 domains and graphite or h-BN represents the major contribution to the load L[7]. Thus, we can estimate the magnitude of the COF, μ, by using:

$$\mu = F_{r0}/L_0$$

$$L_0 = G \cdot A$$

where G＝1.131±0.014 GPa is the critical adhesive pressure between graphite and MoS_2 sheets[18]; and A is the area of the domain. From Fig. S3**a**, the area of our largest MoS_2 domain on graphite is A = 15 μm^2 and the friction force is $F_{r0} = 44.15$ nN giving the adhesive force $L_0 = 16.97$ mN and the COF of the MoS_2/graphite heterostructure interfaces as $\mu_{MG} = 2.6\times10^{-6}$. This value is almost two orders of

magnitude smaller than those reported in previous studies[7,19,20]. For the MoS_2/h-BN heterostructure, according to Fig. S3**b,** the COF value is around $\mu_{MB} = 2.29\times10^{-6}$, similar to MoS_2/graphite.

To further explore the twist-angle dependence of superlubricity in large lattice mismatch heterostructures, we performed the friction test on the MoS_2/graphite heterostructure with different twist angles. Although the heterostructures can be rotated to any twist angle[21], they are only stable at large twist angles during sliding. We compare the friction force between aligned structures (0°/60°) and large twist angles of different MoS_2 domains. As shown in Fig.3**c,** the measured friction forces from MoS_2/graphite heterostructures before and after twisting show no angular dependence. This phenomenon is due to the fact that the in-plane interface friction force is almost zero even at 0° due to incommensurability, and the influence of the twist angle on the friction force has a negligible contribution to the total friction force. (please refer to Supplementary Note 3 for more details).

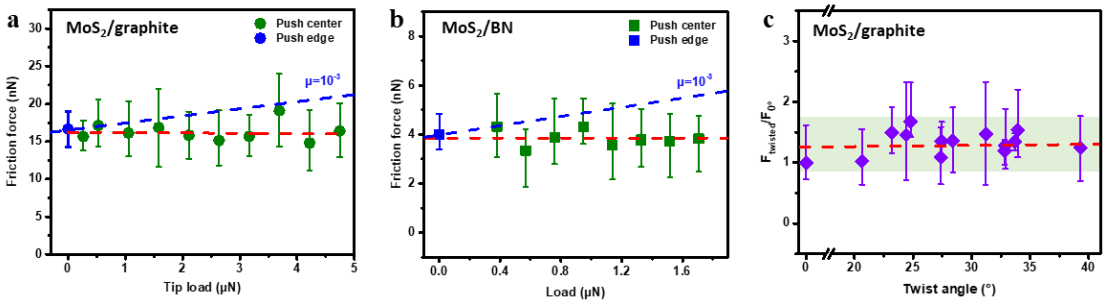

Fig. 2 | Superlubricity of MoS_2/graphite and MoS_2/h-BN heterostructure interfaces. a and **b** Friction force as a function of the tip load of MoS_2/graphite and MoS_2/h-BN heterostructures, obtained by AC200TS and AC240TS tips under N_2 gas environment. The red dashed lines are the fits, the blue dashed line shows the limit of superlubricity. **c** The ratio of friction force before and after twisting of the MoS_2/graphite heterostructure. $F_{0°}$ and $F_{Twisted}$ are the friction forces of a MoS_2 domain before (aligned) and after twisting. The red dashed line is the fit.

Edge pinning effect of large lattice mismatch vdW heterostructures

Although the interface COFs of MoS_2/graphite and MoS_2/h-BN heterostructure interfaces are small, there is still a constant friction force F_{r0} independent of load. Previous results pointed out that the friction force could be affected by many parameters, such as edges, interface steps, and contaminations[22-24]. To determine the origin of this constant friction force, we define two parameters: shear strength S and domain edge pinning strength E. Considering the finite size of our samples, S and E

are defined as follows:

$$S = F_r/A$$

$$E = F_r/P,$$

where A and P are the area and the perimeter of domains, respectively. We can expect three situations: 1) the in-plane interface sliding resistance predominantly contributes to the friction force and S is thus constant; 2) the in-plane interface friction is negligible and the edge pinning effect dominates the friction process and E is constant; 3) if both effects contribute significantly to the friction force, then both S and E cannot be constant.

We first measured the friction force of the aligned heterostructure samples with various contact areas under a dry N_2 atmosphere. The results are consistent even though different tips were used (Fig. S3), suggesting that our calibration method is very reliable. Fig. 3a shows a plot of the shear strength (S) of the MoS_2/graphite heterostructure as a function of domain area (A), clearly revealing a non-constant S. In contrast, when we plot the data as E vs. P, as shown in Fig. 3**b**, the edge pinning strength E is constant with $E = 1.99^{+0.35}_{-0.25}$ nN/μm. These results indicate that the interface (in-plane) friction within MoS_2/graphite is negligible, and the edges of the MoS_2 domains are pinned to the surface of graphite. MoS_2/h-BN exhibits similar behavior, as shown in Fig. 3c and 3d, where $E = 1.94^{+0.80}_{-0.59}$ nN/μm being very close to that of MoS_2/graphite. It is also worth noting that the thickness of MoS_2 domains has no apparent effect on the friction force due to the negligible interface friction (please also refer to Fig. S2**d**). As described above, the friction force of large lattice mismatch MoS_2/graphite and MoS_2/h-BN heterostructures mainly comes from the pinned edges. Therefore, the friction coefficient of infinite interfaces should be significantly lower than 10^{-6}.

The behavior of the aligned graphene/h-BN heterostructure, which has a small lattice mismatch (1.8%), is different from the MoS_2/graphite and MoS_2/h-BN heterostructures. From Fig. 3**e** and 3**f**, we can see that the shear strength of the graphene/h-BN heterostructure is constant and equal to $S = 2.20 \pm 0.39$ MPa, suggesting that the in-plane interface friction is dominant. The dominance of in-plane friction in graphene/h-BN can be understood by considering its commensurate nature at small twist angles, where moiré superlattice can always be found [14,25,26].

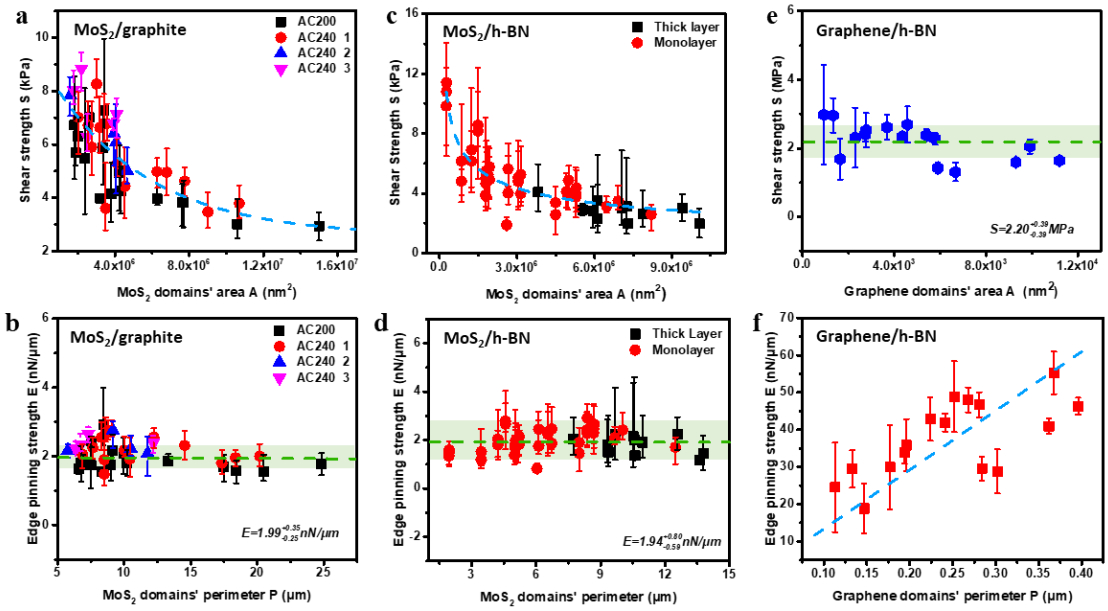

Fig. 3 | Source of friction for three different heterostructure interfaces. a and **b** are plots of friction characterization of MoS_2/graphite as a function of domain area A and perimeter P, respectively. **c** and **d** are similar plots for MoS_2/h-BN. **e** and **f** Friction characterization of graphene/h-BN as a function of A and P.

Simulation results of edge pinning effect of MoS_2/graphite heterostructure

To understand the origin of the edge pinning effect for the MoS_2/graphene heterostructure, we performed a set of molecular dynamics (MD) simulations. The computational setups are illustrated in Fig. 4**a** and **b**. We considered triangular MoS_2 flakes with different side lengths ranging from 2 to 20 nm. Since no reactive force fields are available for the MoS_2/graphene system, we described the interlayer interactions by means of Stillinger-Weber[27] and AIREBO[28] potentials for MoS_2 and graphene, respectively. The interlayer interactions are modeled via a Lennard-Jones potential, which we recently parameterized[29] using ab initio data. According to this potential, the critical adhesive pressure between MoS_2 and graphite is G＝1.20 GPa, which is in good agreement with both experiments and *ab initio* calculations[18]. All systems have been equilibrated at room temperature, after which non-equilibrium simulations have been performed by applying a constant speed protocol and calculating the lateral force acting on the flake. For more details, please refer to the Methods section.

Fig. 4 summarizes the simulation results. The shear strength (S) and the edge pinning strength (E) are reported as a function of MoS_2 domain area (A) and perimeter (P), respectively. As shown in Fig. 4**c**, S presents a decreasing profile as A increases,

while E is almost constant. We also calculate the shear strength of the infinite heterostructure, $S_{infinite}$= 4.95 kPa, which is at least one order of magnitude smaller than that of our finite heterostructures. These trends are consistent with the experimental observations. To get a more in-depth insight into the underlying mechanisms, we analyzed the results in terms of structural and energetical parameters. Fig. 4**d** reports the map of the atomic root mean square displacement (RMSD) with respect to the equilibrium positions for different atomic layers of MoS_2, and averaged over the MD trajectory. The mean displacement of edge atoms is significantly larger than for center atoms. Mo-S bond length data of the edge and center region in Fig. S4**a** also shows that edge atoms have both a larger bond length and broader distribution. Potential energy maps of different atom types within the MoS_2 layer (Fig. 4**e)** show that the edge S atoms have higher potential energy than S center atoms. Edge Mo atoms also present a similar trend but not as significant as for S atoms (please also refer to potential energy data in Fig.S4**c** and **d**). For the kinetic energy maps in Fig.4**f**, there is no apparent difference between edge atoms and center atoms.

The MD simulations indicate that, during sliding, the edge atoms are more "active" and present more energetic distortions, absorbing and dissipating more energy than the center atoms, providing the greatest contribution to the friction force. Indeed, in Fig. S5, we observe more pronounced lattice distortions at the edges using high-resolution transmission electron microscopy, which supports the simulation results.

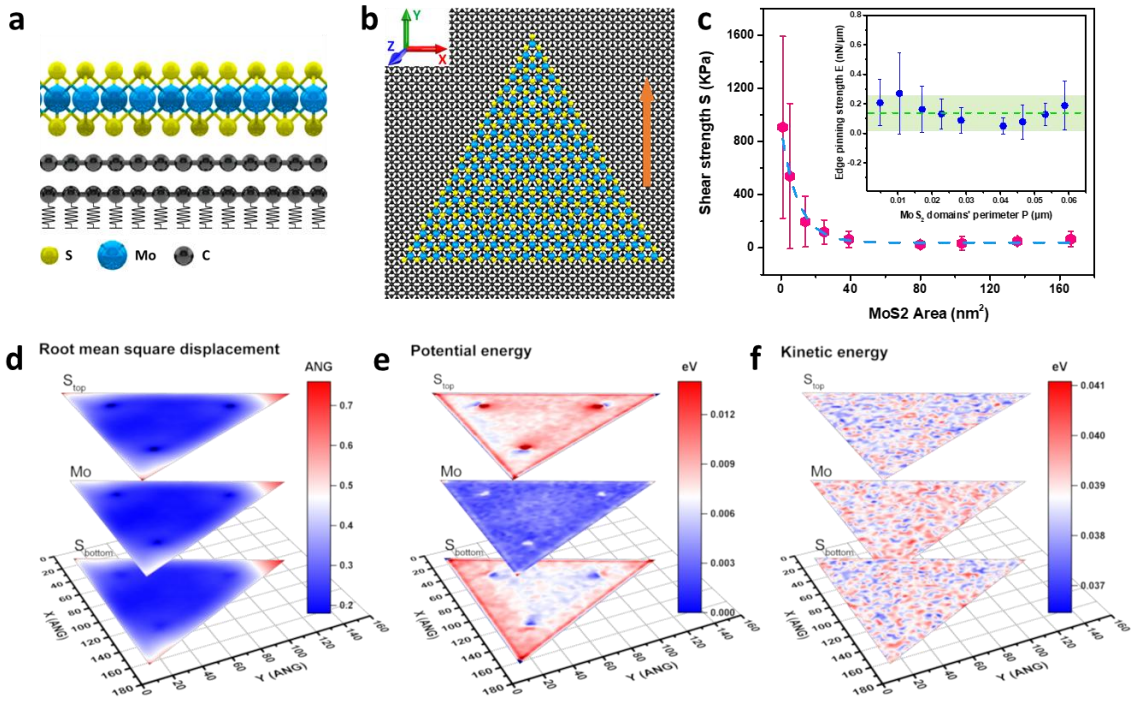

Fig. 4 | MD simulation results of a MoS_2 flake sliding on graphite. a and **b** Side and top views of the MD computational setup, respectively. **c** Calculated shear strength as a function of MoS_2 flake area; the inset shows the calculated edge pinning strength as a function of MoS_2 flakes' perimeter. **d** Root mean square displacement maps of different atomic layers in the MoS_2 flake calculated with respect to the optimized geometry for a typical trajectory (flake size ~ 16 nm). **e** and **f** Per-atom average potential and kinetic energy maps of different atomic layers in the MoS_2 flake, respectively. For the potential energy, values are reported as the difference with respect to the optimized system.

Step pinning effect at MoS_2/graphite heterostructure interfaces.

We have found experimentally that substrate steps can impede the sliding of MoS_2 domains even when they only have the height of a graphene monolayer (~0.4 nm). As shown in Fig. 5**a**, the friction force increases almost tenfold when the MoS_2 domains approach the atomic height graphite step. The interface step pinning strength in Fig.5**a** is ~100 nN/μm, which is two orders of magnitude larger than the edge pinning strength mentioned above. Therefore, the friction force will rise dramatically if interface steps are present, and the superlubricity phenomenon will disappear. We also used MD simulations to monitor the friction force when a MoS_2 flake is pushed toward a graphite step with different angles with respect to the sliding direction, as shown in Fig. 5**b** and **c**. From Fig. 5**c**, we can see that, regardless of the orientation of the step, all profiles show a qualitatively similar behavior; the friction force will rise several times when the MoS_2 layer approaches the step. However, this increase in friction force is smaller than that observed in experiments. The difference between

simulations and experiments can be ascribed to the fact that our model accounts only for non-bonded vdW interactions between flake and substrate (i.e., the model does not allow the formation of chemical bonds between MoS_2 and graphene atoms). Previous works show that chemical bonds on graphite steps have a strong influence on the friction force[30], so we attribute the step pinning effect to the interaction between the MoS_2 layer and the free chemical bonds on the graphite step.

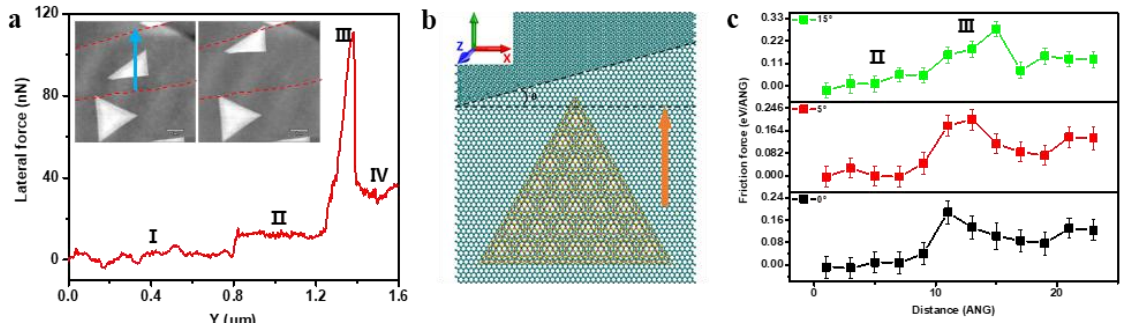

Fig. 5 | Effects of interface steps on friction force. a Lateral force measurements when pushing one MoS_2 domain across a monolayer step of graphite. The red dashed line marks the graphite step, and the blue arrow shows the tip route. The Ⅰ, Ⅱ, Ⅲ, Ⅳ tags the different stages of tip movement: Ⅰ, the tip is moving on graphite; Ⅱ, the tip is pushing the MoS_2 domain; Ⅲ, the MoS_2 domain is moving across the step of graphite; Ⅳ, the MoS_2 domain locks on the step and the tip jump onto the MoS_2 surface. **b** MD computational setup. The dashed line marks the graphite step and the direction normal to the sliding direction (orange arrow). **c** Average friction force experienced by the MoS_2 flake as a function of the distance traveled. The Ⅱ, Ⅲ mark the same stages as **a**.

Conclusion

In conclusion, we demonstrated that large lattice mismatch MoS_2/graphite and MoS_2/h-BN heterojunction interfaces provide ultralow coefficients of friction, ~10^{-6}, without any twist angle dependence. Both experiments and molecular dynamics calculations indicated that pinned edges and interface steps in MoS_2/graphite and MoS_2/h-BN heterojunctions dominate the friction process, whereas small lattice mismatch in graphene/h-BN results in a significant contribution to the interface friction. Our results show that the large lattice mismatch of 2D heterojunctions and absence of interface steps are key components to designing a near-frictionless sliding pair.

Methods

Sample preparation. MoS_2 domains were grown by three-temperature-zone chemical

vapor deposition (CVD). S (Alfa Aesar, 99.9%, 4 g) and MoO_3 (Alfa Aesar, 99.999%, 50 mg) powders were used as sources, loaded separately in two inner tubes and placed at zone-I and Zone-II, respectively. Substrates were loaded in zone-III. During the growth, Ar/O_2 (gas flow rate: 75/3 sccm) was flowed as carrying gases and temperatures for the S-source, MoO_3-source and wafer substrate are 115 ℃, 530 ℃, and 930 ℃, respectively. Graphite and h-BN substrates were mechanically exfoliated from HOPG, Graphenium graphite (*Manchester Nanomaterials*), h-BN are used as substrates in this experiment.

PECVD Growth of graphene/h-BN heterostructure. h-BN flakes were prepared by mechanical exfoliation of h-BN crystals onto 300-nm SiO_2/Si substrate by Scotch tape. Before growth, the substrate was annealed in hydrogen at 400 °C for 30 min to remove tape residues. Subsequently, the epitaxial growth was carried out by R-PECVD at a substrate temperature of ~500 °C with pure CH_4 as the carbon source, and the gas pressure and plasma power were 0.2 torr and 100 W, respectively. The growth period was about 1.5h.

Sample Characterizations. AFM measurements were performed on Asylum Research Cypher S with AC240TS-R3 and AC200TS-R3 tips. PL and Raman characterizations were performed in a Horiba Jobin Yvon LabRAM HR-Evolution Raman system. The laser wavelength is 532 nm. SAED was performed in a TEM (Philips CM200) operating at 200 kV.

Environment control and Cantilever calibration. We placed Cypher S in a specialized glove box. Under dry N_2 conditions, O_2 and H_2O were below 0.5ppm. We used standard Sader's method to calibrate the cantilever in the vertical direction and a non-contact method for the lateral direction[31,32]. During our measurements, two types of silicon AFM tips (AC200TS-R3 and AC240TS-R3) with different mechanical properties were used. The velocity of the tips is 0.6μm/s. For more details, please see Supplementary Note 2.

Simulation. Crystal structures for MoS_2[33] and graphite[34] were retrieved from the Crystallography Open Database[35]. The unit cell of bulk MoS_2 was transformed into a monolayer structure by removing half of the atoms in the cell and adding 20 Å of vacuum along the direction perpendicular to the basal plane in order to avoid interactions between images. The structure was replicated in the *a* and *b* directions and triangular flakes with zigzag edges (ending with sulfur atoms) and varying sides from 20 to 200 Å were cut out. The flake structures were then optimized according to

the Stillinger-Weber potential for MoS_2[27]. A bilayer graphene structure was obtained in a similar way and then optimized using the AIREBO decription[28]. The flake structures were then placed on top of the substrates within an orthogonal cell and finally optimized via energy minimizations with the conjugate gradients method. The interlayer interactions were modeled using a pure Lennard-Jones potential. Since the parameterization available in literature[27] proved to be unsuitable for describing the stacking interaction of MoS_2 and graphene correctly, we refined the actual parameters using Density Functional Theory calculations as a reference. More details about the procedure can be found elsewhere[29]. All structures were then thermalized at 300 K for 50 ps using a Nosé-Hoover thermostat[36,37]. In order to obtain results with statistical significance, ten independent runs were performed for each setup by initializing the atomic velocities to the target temperature with different seeds for the random number generator. After this, sliding simulations of 2 ns were carried out by imposing a constant speed of 1 m/s to three atoms (whose relative positions were not allowed to change) within the top S layer and equidistant from the corners of the flake's. In order to prevent the whole system from moving, the positions of the C atoms belonging to the bottommost graphene layer were tethered to their initial positions by applying harmonic potentials with a spring constant of 0.3 N/m. Forces acting on the externally controlled group of atoms and along the sliding direction were stored and then averaged over the production trajectory. Final averages and standard deviations over the ten independent trajectories were then calculated and reported in the main text. For the simulations involving the graphitic step, in order to mimic the AFM setup, the motion of the MoS_2 flake was obtained by imposing a constant speed to three atoms at the center of the flake edge opposite to the graphitic step. For all MD simulations a time step of 0.2 fs was employed. All calculations were carried out using the LAMMPS package[38].

Acknowledgments

We are grateful to B. J. Irving for carefully reading the manuscript. G.Z. thanks the National Science Foundation of China (NSFC, grant nos 11834017 and 61888102) and the Strategic Priority Research Program of CAS (grant no. XDB30000000) for their support. M.L. thanks the ESI Fund and the OPR DE International Mobility of Researchers MSCA-IF III at CTU in Prague (no.

CZ.02.2.69/0.0/0.0/20_079/0017983) for their support. L.D. gratefully acknowledges the financial support from the Academy of Finland (grant no. 333099). D.S. thanks the support from NSFC (grant no. 61734001). K.W. and T.T. acknowledge support from the Elemental Strategy Initiative conducted by the MEXT, Japan, A3 Foresight by JSPS and the CREST (JPMJCR15F3), JST. M.L., P.N. and T.P. acknowledge support from the project Novel Nanostructures for Engineering Applications CZ.02.1.01/0.0/0.0/16_026/0008396. This work was supported by the Ministry of Education, Youth and Sports of the Czech Republic through the e-INFRA CZ (ID:90140). T.P., V.E.P.C. and A.S. acknowledge support from the European Union's Horizon 2020 research and innovation program under grant agreement no. 721642: SOLUTION. The data and materials are available from the corresponding authors upon request. The authors acknowledge the use of the IRIDIS High Performance Computing Facility, and associated support services at the University of Southampton, in the completion of this work.

Author contributions

G.Z. designed the research; M.L. performed the AFM measurements and data analysis; L.D., H.Y., Z.W performed the sample growth, TEM and spectroscopic characterizations; L.G. performed TEM; P.N., V.E.P.C and A.S performed the MD simulations; M.L., P.N. and G.Z wrote, and all authors commented on the manuscript.

References

1 Holmberg, K., Andersson, P. & Erdemir, A. Global energy consumption due to friction in passenger cars. *Tribol Int* **47**, 221-234, doi:https://doi.org/10.1016/j.triboint.2011.11.022 (2012).

2 Holmberg, K. & Erdemir, A. Influence of tribology on global energy consumption, costs and emissions. *Friction* **5**, 263-284, doi:10.1007/s40544-017-0183-5 (2017).

3 Shinjo, K. & Hirano, M. Dynamics of Friction - Superlubric State. *Surf Sci* **283**, 473-478, doi:Doi 10.1016/0039-6028(93)91022-H (1993).

4 Geim, A. K. & Grigorieva, I. V. Van der Waals heterostructures. *Nature* **499**, 419-425, doi:10.1038/nature12385 (2013).

5 Dienwiebel, M. *et al.* Superlubricity of graphite. *Phys Rev Lett* **92**, 126101, doi:10.1103/PhysRevLett.92.126101 (2004).

6 Zheng, Q. *et al.* Self-retracting motion of graphite microflakes. *Phys Rev Lett* **100**, 067205, doi:10.1103/PhysRevLett.100.067205 (2008).

7 Li, H. *et al.* Superlubricity between MoS2 Monolayers. *Adv Mater* **29**, 1701474-n/a, doi:10.1002/adma.201701474 (2017).

8 Filippov, A. E., Dienwiebel, M., Frenken, J. W., Klafter, J. & Urbakh, M. Torque and twist against superlubricity. *Phys Rev Lett* **100**, 046102, doi:10.1103/PhysRevLett.100.046102 (2008).

9 Ribeiro-Palau, R. *et al.* Twistable electronics with dynamically rotatable heterostructures. *Science* **361**, 690-693, doi:10.1126/science.aat6981 (2018).
10 Song, Y. *et al.* Robust microscale superlubricity in graphite/hexagonal boron nitride layered heterojunctions. *Nature Materials* **17**, 894-899, doi:10.1038/s41563-018-0144-z (2018).
11 Wang, D. *et al.* Thermally Induced Graphene Rotation on Hexagonal Boron Nitride. *Phys Rev Lett* **116**, 126101, doi:10.1103/PhysRevLett.116.126101 (2016).
12 Yu, H. *et al.* Precisely Aligned Monolayer MoS2 Epitaxially Grown on h-BN basal Plane. *Small* **13**, 1603005-n/a, doi:10.1002/smll.201603005 (2017).
13 Du, L. J. *et al.* Modulating PL and electronic structures of MoS2/graphene heterostructures via interlayer twisting angle. *Applied Physics Letters* **111**, doi:Artn 263106 10.1063/1.5011120 (2017).
14 Yang, W. *et al.* Epitaxial growth of single-domain graphene on hexagonal boron nitride. *Nature Materials* **12**, 792, (2013).
15 Radisavljevic, B., Radenovic, A., Brivio, J., Giacometti, V. & Kis, A. Single-layer MoS2 transistors. *Nat Nanotechnol* **6**, 147-150, doi:10.1038/nnano.2010.279 (2011).
16 Liao, M. *et al.* Twist angle-dependent conductivities across MoS2/graphene heterojunctions. *Nature Communications* **9**, 4068, doi:10.1038/s41467-018-06555-w (2018).
17 Müser, M. H. in *Fundamentals of Friction and Wear on the Nanoscale NanoScience and Technology* (eds Enrico Gnecco & Ernst Meyer) Ch. Chapter 11, 209-232 (Springer International Publishing, 2015).
18 Li, B. *et al.* Probing van der Waals interactions at two-dimensional heterointerfaces. *Nature Nanotechnology*, doi:10.1038/s41565-019-0405-2 (2019).
19 Martin, J. M., Donnet, C., Lemogne, T. & Epicier, T. Superlubricity of Molybdenum-Disulfide. *Physical Review B* **48**, 10583-10586, doi:DOI 10.1103/PhysRevB.48.10583 (1993).
20 Berman, D., Deshmukh, S. A., Sankaranarayanan, S. K., Erdemir, A. & Sumant, A. V. Friction. Macroscale superlubricity enabled by graphene nanoscroll formation. *Science* **348**, 1118-1122, doi:10.1126/science.1262024 (2015).
21 Liao, M. *et al.* Twist angle-dependent conductivities across MoS 2/graphene heterojunctions. *Nature communications* **9**, 4068 (2018).
22 Dietzel, D., Feldmann, M., Schwarz, U. D., Fuchs, H. & Schirmeisen, A. Scaling laws of structural lubricity. *Phys Rev Lett* **111**, 235502, doi:10.1103/PhysRevLett.111.235502 (2013).
23 de Wijn, A. S. (In)commensurability, scaling, and multiplicity of friction in nanocrystals and application to gold nanocrystals on graphite. *Physical Review B* **86**, 085429, doi:10.1103/PhysRevB.86.085429 (2012).
24 Muser, M. H., Wenning, L. & Robbins, M. O. Simple microscopic theory of Amontons's laws for static friction. *Phys Rev Lett* **86**, 1295-1298, doi:10.1103/PhysRevLett.86.1295 (2001).
25 Yankowitz, M. *et al.* Emergence of superlattice Dirac points in graphene on hexagonal boron nitride. *Nature Physics* **8**, 382, doi:10.1038/nphys2272 (2012).
26 Wang, E. *et al.* Gaps induced by inversion symmetry breaking and second-generation Dirac cones in graphene/hexagonal boron nitride. *Nature Physics* **12**, 1111 (2016).
27 Ding, Z. W., Pei, Q. X., Jiang, J. W., Huang, W. X. & Zhang, Y. W. Interfacial thermal conductance in graphene/MoS2 heterostructures. *Carbon* **96**, 888-896, doi:10.1016/j.carbon.2015.10.046 (2016).
28 Brenner, D. W. *et al.* A second-generation reactive empirical bond order (REBO) potential energy expression for hydrocarbons. *J Phys-Condens Mat* **14**, 783-802, (2002).
29 Andrea Silva, V. E. P. C., Tomas Polcar, Denis Kramer, Paolo Nicolini. Exploring the stability of twisted van der Waals heterostructures. doi:arXiv:2001.05298 (2020).
30 Chen, Z., Khajeh, A., Martini, A. & Kim, S. H. Chemical and physical origins of friction on surfaces with atomic steps. *Sci Adv* **5**, eaaw0513, doi:10.1126/sciadv.aaw0513 (2019).
31 Sader, J. E., Chon, J. W. M. & Mulvaney, P. Calibration of rectangular atomic force microscope cantilevers. *Rev Sci Instrum* **70**, 3967-3969, doi:Doi 10.1063/1.1150021 (1999).
32 Wagner, K., Cheng, P. & Vezenov, D. Noncontact method for calibration of lateral forces in scanning force microscopy. *Langmuir* **27**, 4635-4644, doi:10.1021/la1046172 (2011).
33 Schonfeld, B., Huang, J. J. & Moss, S. C. Anisotropic Mean-Square Displacements (Msd) in Single-Crystals of 2h-Mos2 and 3r-Mos2. *Acta Crystallogr B* **39**, 404-407, doi:Doi 10.1107/S0108768183002645 (1983).
34 Zemann, J. Crystal structures, 2nd edition. Vol. 1 by R. W. G. Wyckoff. *Acta Crystallographica*

18, 139-139, doi:10.1107/S0365110X65000361 (1965).
35 Grazulis, S. *et al.* Crystallography Open Database (COD): an open-access collection of crystal structures and platform for world-wide collaboration. *Nucleic Acids Res* **40**, D420-D427, doi:10.1093/nar/gkr900 (2012).
36 Nose, S. A Unified Formulation of the Constant Temperature Molecular-Dynamics Methods. *J Chem Phys* **81**, 511-519, doi:Doi 10.1063/1.447334 (1984).
37 Hoover, W. G. Canonical Dynamics - Equilibrium Phase-Space Distributions. *Phys Rev A* **31**, 1695-1697, doi:DOI 10.1103/PhysRevA.31.1695 (1985).
38 Plimpton, S. Fast Parallel Algorithms for Short-Range Molecular-Dynamics. *J Comput Phys* **117**, 1-19, doi:DOI 10.1006/jcph.1995.1039 (1995).